Heliyon 10 (2024) e40750

Contents lists available at ScienceDirect

Heliyon

journal homepage: www.cell.com/heliyon

Research article

Synthesis and characterization of machine learning designed TADF molecules

Weimei Shi [a,c], Yan Li [d], Ziying Zhang [e], Zheng Tan [a,b,c,*], Shiqing Yang [a]

[a] Postdoctoral Innovation Practice Base, Chengdu Polytechnic, 83 Tianyi Street, Chengdu, Sichuan, 610041, PR China
[b] State Key Laboratory of Electronic Thin Films and Integrated Devices, University of Electronic Science and Technology of China, Chengdu, 610054, PR China
[c] Sichuan Provincial Engineering Research Center of Thermoelectric Materials and Devices, Chengdu, Sichuan, 610041, PR China
[d] Xiyuan Quantitative Technology, 388 Yizhou Road, Chengdu, Sichuan, 610000, PR China
[e] Guangzhou Yinfo Information Technology, 2 Ruyi Road, Panyu District, Guangzhou, 511431, PR China

ARTICLE INFO

Keywords:
TADF molecules
machine learning design
Structural characterization
Delayed fluorescence properties

ABSTRACT

In this study, we present a novel approach to the development of thermally activated delayed fluorescence (TADF) molecules with potentials for organic light-emitting diode (OLED) applications, leveraging machine learning (ML) algorithms to guide the materials design process. Recognizing the imperative for high-efficiency, low-cost emissive materials, we integrated ML driven models with experimental characterization to expedite the discovery of TADF compounds. Initially, a database of ML-designed TADF molecules was employed, with samples being approved to possess optimized photophysical properties. The proposed molecules were synthesized using palladium-catalyzed coupling reactions. Subsequent characterization of these molecules utilized a suite of analytical methods, including nuclear magnetic resonance (NMR) spectroscopy, photoluminescence (PL) spectroscopy, and transient PL decay etc., to confirm their structural integrity and evaluate their performance metrics. The photophysical analysis revealed notable emission efficiencies and significant delayed fluorescence characteristics in solution phases, underscoring the potential of ML-designed TADF molecules. Theoretical validations, through quantum chemical calculations, corroborated the experimental findings, demonstrating the predictive power of our ML models. This interdisciplinary approach not only accelerates the pace of TADF molecule development but also provides a scalable framework for future material innovation especially in the OLED research field.

1. Introduction

In recent years, OLED technology has undergone significant advancements, serving as a catalyst for innovations in high-efficiency and cost-effective lighting and display solutions. At the forefront of this progress is TADF, a critical technology in the OLED sector, have been extensively studied in the past decade due to their huge potential in making high efficiency OLED devices [1–7]. Moreover, the design and synthesis of TADF molecules are central to enhancing the performance, durability, and sustainability of OLED systems [8].

Conventional methods for designing TADF molecules often rely on repetitive experimental approaches and subjective insights, resulting in a time-consuming and resource-intensive process. With the development of time-dependent density functional theory

* Corresponding author. Postdoctoral Innovation Practice Base, Chengdu Polytechnic, 83 Tianyi Street, Chengdu, Sichuan, 610041, PR China
E-mail address: zhengtan1983@hotmail.com (Z. Tan).

https://doi.org/10.1016/j.heliyon.2024.e40750
Received 13 June 2024; Received in revised form 3 November 2024; Accepted 26 November 2024
Available online 28 November 2024

(TDDFT) which is known to provide reasonably accurate descriptions of excited state properties, it has seen high-throughput screenings using TDDFT to explore the search space of TADF molecules [9,10]. Furthermore, recent involvement of ML techniques in the materials science has significantly accelerate the materials discovery, resulting in novel structure design and property optimization in a far more efficient way, compared to the trial-and-error approach [11,12]. In the case of TADF design, both property predictions and structure inverse design based on deep learning have been extensively explored. Tan et al. [13] have applied deep neural network, graph convolutional network, recurrent neural network, message passing neural network and SchNet models to predict the TADF photophysical properties including the excited state energies and oscillator strengths; while they further found that by extending the molecular torsional profiles, the predictive accuracies of oscillator strengths can be additionally improved. Inverse design utilizing adversarial autoencoder [14] (AAE) has also been employed to investigate the possible molecular structure by creating an 'image' dataset from the original TADF samples. By combining the fine screening procedure, Tan et al. [14] have eventually identified 19 TADF molecules with qualified photophysical properties (where the calculated singlet−triplet energy gaps and spin−orbital couplings satisfy the prescribed criteria).

The current research leverages ML algorithms to direct the design and synthesis of TADF molecules. A database of ML-designed TADF molecules is employed, with the samples being created from adversarial generation and fine screening processes [14]. Two of the molecules are selected and synthesized through the palladium-catalyzed cross-coupling. To validate the newly synthesized molecules, a suite of analytical tools—including Nuclear Magnetic Resonance (NMR) spectroscopy, Photoluminescence (PL) spectroscopy, transient PL decay and PL quantum yield measurement—is used to confirm their structures and assess performance metrics. The newly synthesized molecules are tested mainly in solution phases, demonstrating notable luminescent efficiency and delayed fluorescent behaviours. The work emphasizes the integral role of ML in the development of TADF molecules, while the artificially created samples can possess desired electronic structure, satisfactory photophysical properties which can also be validated

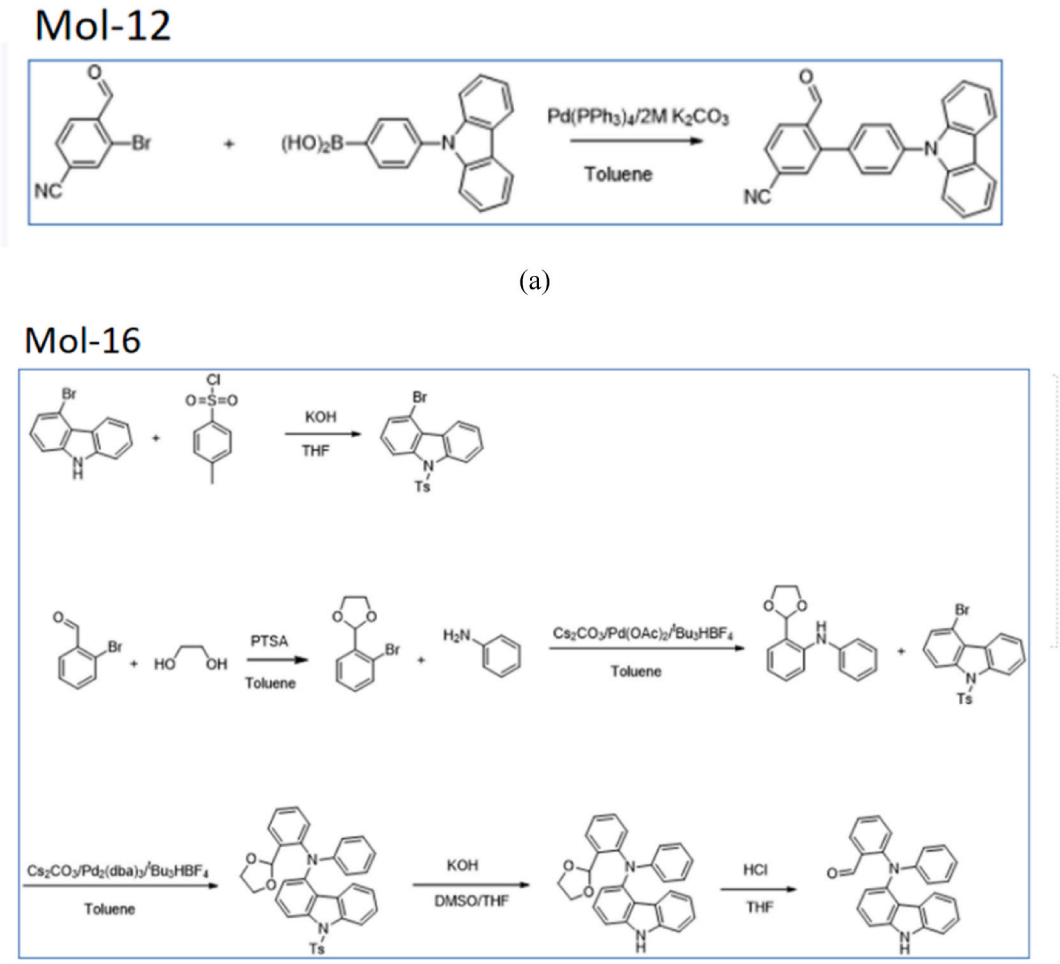

Fig. 1. Synthesis of (a) mol_12 and (b) mol_16.

experimentally. It implies huge potential of machine learning in expediting material innovation in both theoretical design and experimental justification, offering significant opportunities for intelligent development of the visual display technologies.

The paper is organized as below. The second section demonstrates the methodology including the synthetic procedures for making the selected molecules, the instrumentation and the implementation details for quantum chemical calculations. The results and discussion section presents the empirical results and discusses the main findings of our study. A conclusion is drawn in the end.

2. Methodology

2.1. Synthetic procedures

2.1.1. Synthesis of mol_12

The synthesis of mol_12 employs a palladium-catalyzed cross-coupling reaction, which is a well-established method in organic synthesis for forming carbon-carbon bonds [15–19]. The reaction is implemented by combining 10 g of 4-bromo-3-nitrobenzoate with 12 g of nitrogen-containing phenylboronic acid. These reactants are precisely measured to ensure stoichiometric balance and optimal reaction efficiency. The catalyst used in this reaction, palladium tetrakis(triphenylphosphine) ($Pd(PPh_3)_4$), is added in a small amount of 0.5 g, providing the necessary activity to facilitate the coupling process. Additionally, 8 g of potassium carbonate are used as a base, usually in excess, to drive the reaction towards completion.

Toluene is chosen for the reaction solvent in a volume of 300 mL. The reaction mixture is heated to approximately 110 °C, and maintained at reflux for 16 h. This extended duration ensures the completion of the coupling reaction, allowing for the formation of the biaryl bond between the bromo-nitrobenzoate and the phenylboronic acid derivative. When the reaction is finished, the mixture is allowed to cool to room temperature. The product is then isolated via quenching the reaction and purifying through column chromatography.

We perform the ^{1}H NMR spectroscopy to identify the structure of the synthesized molecule, with data being given as: ^{1}H NMR (500 MHz, $CDCl_3$) δ 10.16 (s, 1H), 8.15 (d, $J = 7.5$ Hz, 3H), 7.89 (d, $J = 1.0$ Hz, 1H), 7.82 (d, $J = 8.0$ Hz, 1H), 7.75 (d, $J = 8.0$ Hz, 2H), 7.61 (d, $J = 8.5$ Hz, 2H), 7.49 (d, $J = 8.5$ Hz, 2H), 7.45–7.42 (m, 2H), 7.33–7.30 (m, 2H). We find that the NMR indicated structure fully matches the theoretically designed configuration of mol_12 as shown in Fig. 3.

2.1.2. Synthesis of mol_16

Fig. 1(b) depicts the synthetic pathway for the compound mol_16, detailing a sequence of reactions leading to its formation, including bromination, cross-coupling reactions, and functional group transformations. In the first step, a nucleophilic aromatic substitution is carried out with 5 g of a brominated heteroaromatic compound and 4 g of chloro-tosylate. This reaction uses 3 g of potassium hydroxide dissolved in 120 mL of tetrahydrofuran (THF). The mixture is stirred at room temperature for 4 h, facilitating the replacement of the tosylate group with the nucleophilic aromatic compound, and forming a Ts-protected nitrogen-containing ring structure.

Following this, the Friedel-Crafts alkylation involves 5 g each of bromophenol and an aromatic aldehyde. The catalyst, 2 g of p-toluenesulfonic acid (PTSA), is used in 200 mL of toluene. This reaction is refluxed for 7 h at about 110 °C, the boiling point of toluene. This step results in the formation of an ether linkage between the phenol and aldehyde, advancing the complexity of the molecular framework.

The critical structural features are then established through a palladium-catalyzed coupling reaction. This stage employs 6 g each of a nitrogen-containing heteroaromatic compound and a bromo-substituted intermediate, with a catalyst system comprising 0.5 g of $Pd(OAc)_2$, 3 g of Cs_2CO_3, and 0.5 g of $^tBu_3HBF_4$ in 250 mL of toluene. The reaction mixture is refluxed for 18 h, promoting the formation of an extended polycyclic structure via cross-coupling.

Subsequent deprotection of the nitrogen atom utilizes 5 g of KOH in a 150 mL mixture of DMSO and THF. This mixture is heated to 100 °C and stirred for 12 h, enabling the removal of the Ts group under mild conditions. The final step in the synthesis involves the hydrolysis of the lactone group to a ketone structure, using hydrochloric acid (100 mL of 1M) in THF. The reaction is conducted at 0 °C for 3 h to complete the synthesis of mol_16.

The NMR data is given as: ^{1}H NMR (500 MHz, $CDCl_3$) δ 10.17 (s, 1H), 8.19 (s, 1H), 7.86 (dd, $J = 8.0$, 1.5 Hz, 1H), 7.52–7.47 (m, 2H), 7.38 (d, $J = 8.0$ Hz, 1H), 7.33–7.29 (m, 2H), 7.28–7.25 (m, 2H), 7.24–7.21 (m, 1H), 7.09–7.04 (m, 2H), 6.94–6.88 (m, 2H), 6.72 (d, $J = 7.5$ Hz, 2H). Again, we find that the identified structure is fully consistent with the designed configuration of mol_16 shown in Fig. 3.

2.1.3. Instrumentation and measurements

Nuclear magnetic resonance (NMR) spectra were measured on an Avance III 500 spectrometer (Bruker) and JNM-ECP400 spectrometer (JEOL). NMR chemical shifts are reported in parts per million (ppm) using tetramethysilane as an internal standard (TMS = 0.0 ppm). Elemental analyses were carried out with a Yanaco MT-5 CHN corder. Photoluminescence (PL) spectra of organic solutions were measured with a FluoroMax-4 spectrofluorometer. PL quantum yield was measured by an absolute PL quantum yield measurement system (Hamamatsu Photonics C11347-10). Luminescence lifetime of solutions was measured with a Quan-taurus-Tau system (Hamamatsu Photonics).

Note that the synthesized two molecules (mol_12 and mol_16) are dissolved in toluene, chloroform and hexane respectively, to take the measurement of PL spectroscopy, PL quantum yield and luminescence lifetime. The PL decay profiles of solutions are measured after N_2 bubbling.

2.1.4. Quantum chemical calculations

The TADF candidates are inherited from our previous machine learning design results [14] where 19 molecules are screened out based on the excited-state optimizations and spin−orbital coupling (SOC) calculations. Two candidates are selected for experimental synthesis, while quantum chemical calculations were performed using Gaussian 16 [20] at the level of B3LYP/def2SVP to identify the electronic structure according to the pre-optimized ground-state geometries. The fluorescence spectra of the selected molecules were calculated using the first principles path integral approach implemented in ORCA [21]. The initial (S_1 optimized geometry) and final (ground state optimized geometry) states for the fluorescent transition and their respective Hessian matrices are computed (at the B3LYP/def2SVP level). After the calculations of transition dipole derivatives, the spectra were predicted in terms of a discrete Fourier transform of the transition dipole correlation function, including both the Franck–Condon and Herzberg–Teller (HT) effects [22]. The spectra were broadened using a Voigt function with line widths of 50 cm^{-1} for the Lorentzian component and 250 cm^{-1} for the Gaussian component.

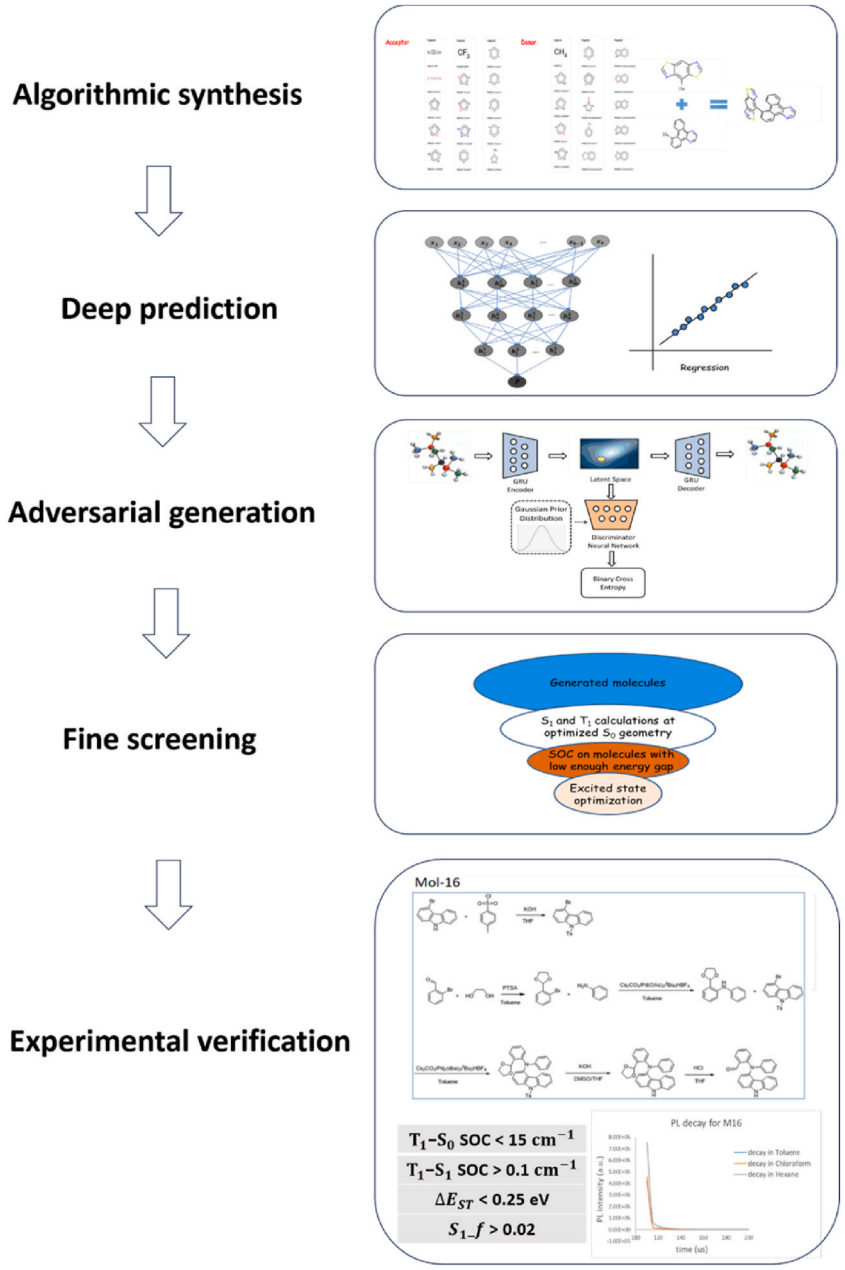

Fig. 2. Machine learning design roadmap for TADF molecules, including modules of algorithmic synthesis, deep prediction, adversarial generation, fine screening and experimental verification.

3. Results and discussion

3.1. Machine learning design roadmap for TADF compounds

Fig. 2 depicts the ML assisted design process for TADF molecules from the theoretical generation to experimental verifications. As referring to our previous publication [14], the process involves the algorithmic synthesis by combining the empirical donor and acceptor fragments via the BRICS rule, deep prediction by constructing the ECFP fingerprint to forecast the excited state properties, adversarial generation by using the AAE model to create artificial molecules that can possess similar photophysical properties with the original samples, and the fine screening to select TADF candidates with satisfactory properties from the generation space. The screening basically goes through a hierarchical process, by conducting high throughput calculations of TDDFT single points, SOC and excited-state optimizations, with gradually raised computational costs.

The final step in Fig. 2 refers to the experimental verification of the screened samples satisfying certain criteria. We prescribe the selection standards as T_1-S_0 SOC <15 cm^{-1}, T_1-S_1 SOC >0.1 cm^{-1}, $\Delta E_{ST} < 0.25$ eV and $S_1 f > 0.02$, in order to guarantee a proper intersystem coupling, a small enough adiabatic gap and a considerable oscillator strength. Two molecules chosen from the qualified TADF candidates are finally synthesized, to experimentally validate the photophysical properties of ML designed species (which constitutes the main theme of the current paper).

3.2. Electronic structure characterization

Table 1 showcases a series of novel molecules designed via the AAE model as potential TADF candidates (as inherited from the results in Ref. [14]), characterized by their electronic and SOC properties. The molecular structures (Fig. 3), ranging from mol_1 to mol_19, exhibit diverse aromatic and heteroaromatic frameworks, all of which are of essentially electron-donor and electron-acceptor

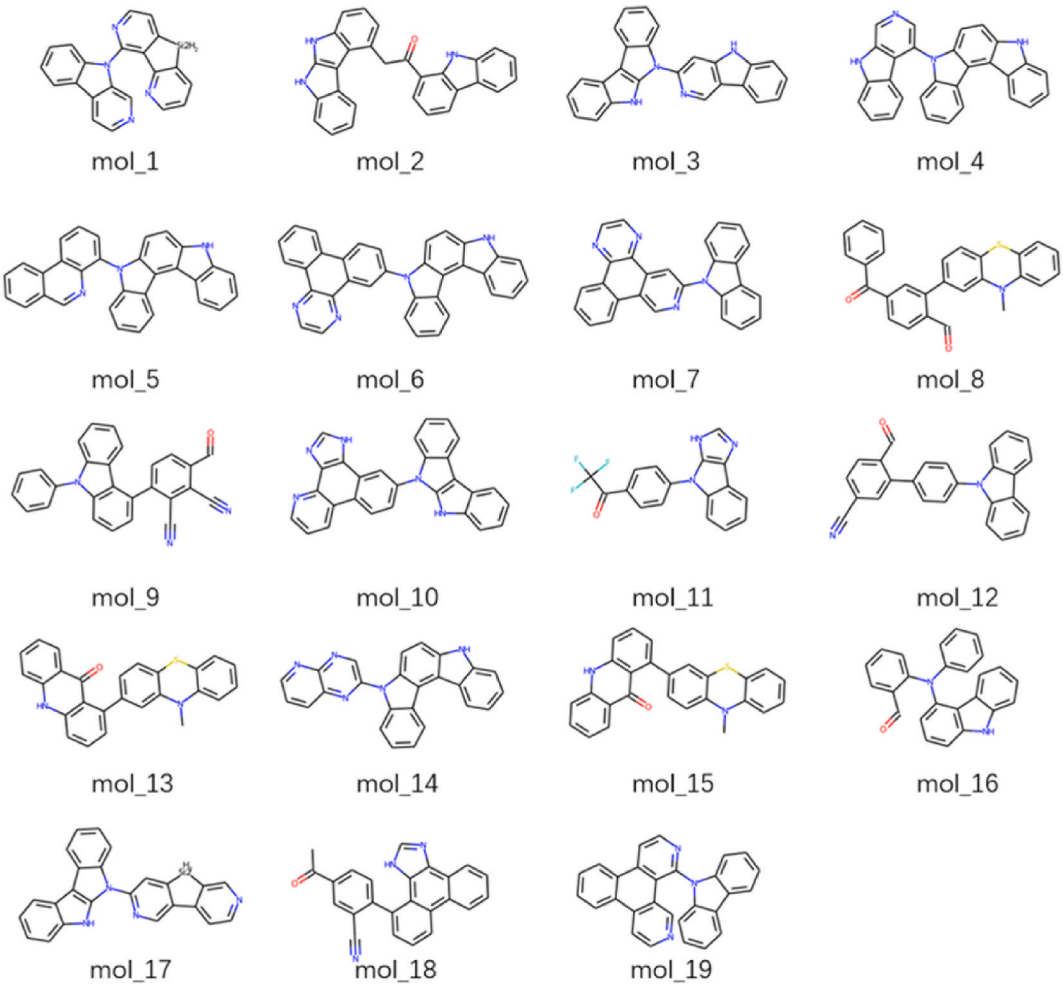

Fig. 3. Machine learning designed molecules with satisfactory quantum chemical properties for the delayed fluorescence.

combinations, as evidenced in the structural depictions. The computed adiabatic singlet-triplet gaps (ΔE_{ST}) indicate the thermally accessible reverse intersystem crossing (rISC) essential for TADF. Notably, all molecules demonstrate ΔE_{ST} smaller than 0.25 eV, which are favorable for efficient TADF. Moreover, the non-negligible SOC constants between T_1 and S_1 states, suggest effective intersystem crossing channels.

Remarkably, the created donor-acceptor configurations substantially mimic the original TADF samples that were fed into the AAE algorithm, implying the efficacy of the adversarial generation in producing reasonable chemical structures with desired photophysical properties. The results affirm the utility of machine learning in the design of TADF materials by enabling the prediction and optimization of critical properties that correlate with photoluminescent performance, pointing towards a tailored approach in the design of TADF emitters.

In the study of molecular electronic structures, frontier orbitals provide profound insight into the photophysics of chemical species. The visualization of the HOMO and LUMO for mol_12 and mol_16, as demonstrated in Fig. 4, elucidates the spatial distribution of the electron density that governs their photophysical behavior. For mol_12 (Fig. 4(a)), both the HOMO and LUMO are highly localized within corresponding molecular moieties, demonstrating diminished orbital overlaps and a significant charge transfer characteristic. It is consistent with the minimized adiabatic gap (ΔE_{ST} = 0.0084 eV without TDA), which is favorable for TADF with augmented photoluminescent performance.

Mol_16 (Fig. 4(b)) exhibits a slightly different pattern, with the HOMO revealing a significant delocalization over the conjugated system while the LUMO shows a more localized character. The distributions point towards a less efficient orbital separation which corresponds to a slightly enhanced B3LYP adiabatic gap (ΔE_{ST} = 0.1579 eV without TDA) computed for mol_16. Compared to mol_12, the observation can theoretically imply a reduced rISC rate and therefore suppressed thermal activation for delayed fluorescence. These differences in frontier orbital characteristics between mol_12 and mol_16 underscore the importance of the electronic configuration in dictating molecular properties.

3.3. Photoluminescence spectroscopy

The fluorescence spectral analysis of molecules mol_12 and mol_16 dissolved in toluene, chloroform, and hexane respectively (see Fig. 5) presents a comprehensive view of solvatochromic shifts that manifest due to solvent-solute interactions. For molecule mol_12, a significant hypsochromic (blue) shift observed in toluene and hexane suggests a decrease in polarity around the fluorophore, influencing the electronic distribution in the excited state. Similarly, mol_16 exhibits the greatest red shift in chloroform compared to toluene and hexane, which could be associated with specific solvent interactions at the excited state, altering the molecular orbital energies due to the enlarged solvent polarity.

These observations for both mol_12 and mol_16 suggest the validity of the machine learning approach in designing reasonable chemical species possessing verifiable fluorescence behaviors in solution phases.

As exhibited in Fig. 6, the fluorescence spectra of molecules mol_12 and mol_16 in chloroform were analyzed, comparing experimental results with theoretical predictions. For mol_12, the experimental spectrum reveals a major peak at approximately 530 nm, with an insignificant shoulder at around 400 nm, and a smaller peak near 700 nm. The theoretical spectrum correlates closely with the

Table 1
Potential TADF candidates designed by machine learning. The listed properties include adiabatic singlet−triplet gaps computed via the B3LYP functional with and without the Tamm−Dancoff approximation (TDA), the T_1S_1 and T_1S_0 SOC Constants at the S_0 Geometry.

Name	SMILES	B3LYP gap (eV)	B3LYP-TDA gap (eV)	T_1S_1 SOC (cm^{-1})	T_1S_0 SOC (cm^{-1})
mol_1	c1cnc2c(c1)[SiH2:2]c1ccnc(-n3c4ccccc4c4ccncc43)c1-2	0.1333	0.0106	0.3239	1.8620
mol_2	O=C(Cc1cccc2[nH]c3[nH]c4ccccc4c3c12)c1cccc2c1[nH]c1ccccc12	0.0163	0.0117	1.8729	7.1232
mol_3	c1ccc2c(c1)[nH]c1c2c2ccccc2n1-c1cc2[nH]c3ccccc3c2cn1	0.1223	0.0980	0.1136	0.7360
mol_4	c1ccc2c(c1)[nH]c1ccc3c(c4ccccc4n3-c3cncc4[nH]c5ccccc5c34)c12	0.1759	0.0798	0.1606	0.1746
mol_5	c1cc2c(cc1)[nH]c1ccc3c(c4ccccc4n3-c3cccc4c3ncc3ccccc34)c12	0.0227	0.0144	0.1703	1.3593
mol_6	c1ccc2c(c1)[nH]c1ccc3c(c4ccccc4n3-c3ccc4c5ccccc5c5nccnc5c4c3)c12	0.0130	0.0117	0.1225	1.0532
mol_7	c1ccc2c(c1)-c1cnc(-n3c4ccccc4c4ccccc43)cc1c1nccnc21	0.0995	0.0926	0.1396	1.6184
mol_8	O=C(c1ccc(C=O)c(-c2ccc3c(c2)Nc2ccccc2S3)c1)c1ccccc1	0.0483	0.0391	0.1507	8.6579
mol_9	O=Cc1ccc(-c2cccc3c2c2ccccc2n3-c2ccccc2)c(C#N)c1C#N	0.1280	0.0367	0.2102	0.7563
mol_10	c1cnc2c(c1)-c1ccc(-n3c4ccccc4c4c5ccccc5[nH]c43)cc1c1[nH]cnc21	0.0082	0.0078	0.2818	0.8635
mol_11	O=C(c1ccc(-n2c3ccccc3c3nc[nH]c23)cc1)C(F)(F)F	0.0070	0.0065	0.1691	1.7473
mol_12	N#Cc1ccc(C=O)c(-c2ccc(-n3c4ccccc4c4ccccc43)cc2)c1	0.0084	−0.0066	0.1288	9.6389
mol_13	CN1c2ccccc2Sc2ccc(-c3cccc4Nc5ccccc5c(=O)c34)cc21	0.2109	0.1751	0.5778	6.8733
mol_14	c1ccc2c(c1)[nH]c1ccc3c(c4ccccc4n3-c3cnc4nccccc4n3)c12	0.0239	0.0204	0.1868	1.7842
mol_15	CN1c2ccccc2Sc2cc(-c3cccc4[nH]c5ccccc5c(=O)c34)ccc21	0.1956	0.1594	0.8683	14.9823
mol_16	O=Cc1ccccc1N(c1cccc2[nH]c3ccccc3c12)c1ccccc1	0.1579	0.1168	0.4755	6.4195
mol_17	c1ccc2c(c1)[nH]c1c2c2ccccc2n1-c1ncc2c(c1)[SiH2:2]c1cnccc1-2	0.0761	0.0616	0.1962	0.7084
mol_18	CC(=O)c1ccc(-c2cccc3c4ccccc4c4nc[nH]c4c23)c(C#N)c1	0.2286	0.1081	0.1208	1.2150
mol_19	c1cc2c(cn1)-c1c(ccnc1-n1c3ccccc3c3ccccc31)c1ccccc12	0.2335	0.0899	0.5408	1.8974

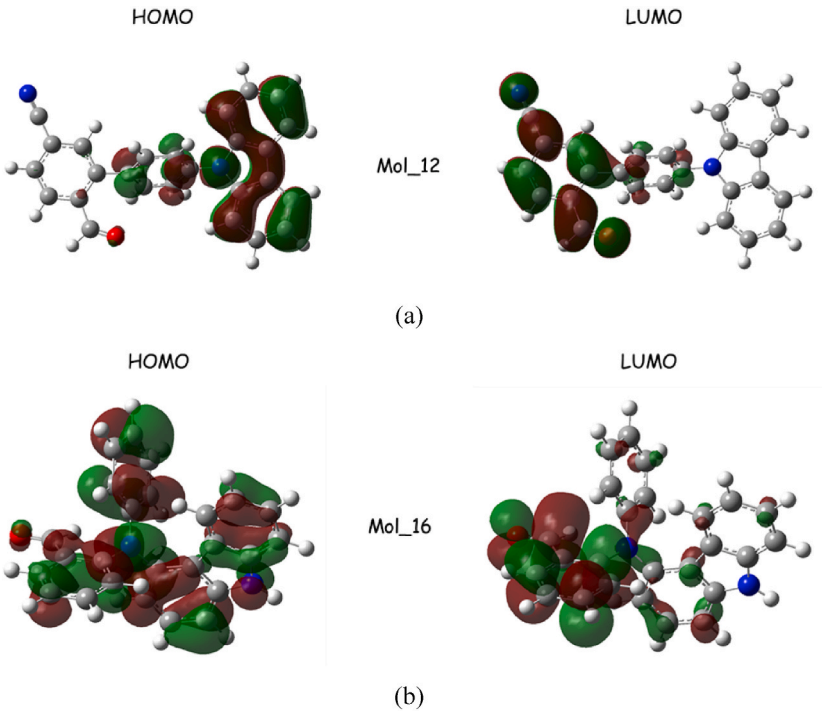

Fig. 4. Frontier orbitals of (a) mol_12 and (b) mol_16 at the optimized S_0 geometries in gaseous phase.

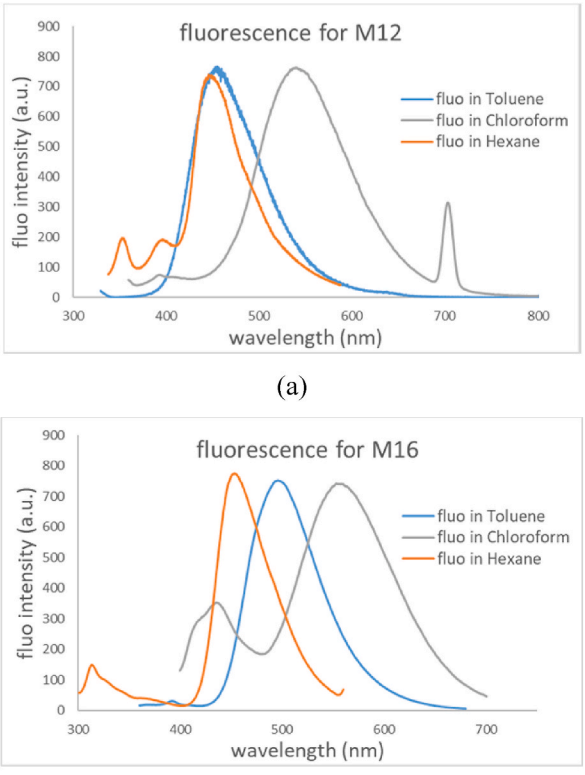

Fig. 5. Fluorescence spectra for (a) mol_12 and (b) mol_16 dissolved in toluene, chloroform and hexane respectively.

experimental data, capturing the main peak's position accurately, indicating the robustness of the C-PCM model in describing the transition energy in solutions. However, the side peaks in the theoretical spectrum at around 600 nm and beyond show less compatibility with the experimental spectrum, implying that refinement might be needed in the theoretical method to account for the complex electronic structure in the excited state. Additionally, the spectral width from theoretical calculations is slightly smaller than the experimental one, probably because the single configurations in S_1 and S_0 considered in the transition may lead to a less efficient inhomogeneous broadening that usually occurs in solution-phase spectra [24].

For mol_16, the experimental spectrum shows a pronounced peak at around 550 nm, which perfectly matches the theoretical main peak. Similar to mol_12, the side peaks and shoulders from the theoretical spectrum exhibit fewer consistency with the experimental measurement, putting challenges on the current model in describing fine structures of the excited state.

Additionally, the vibronic structures in the theoretical spectra for both molecules demonstrate complex interactions between the electronic transitions and nuclear vibrations. For mol_12, the side band deviated from the main peak has a separation of 0.2 eV, which is likely to originate from $\nu 111$ in the normal mode analysis at S_1 geometry. As shown in Fig. 6(b), the vibration is basically dominated by the hydrogen scissoring and the breathing motions of C-C bonds. For mol_16, the normal modes $\nu 96$ and $\nu 103$ at S_1 geometry would correspond to the two side band separations from the main peak (vibronic progressions of 0.17 eV and 0.18 eV respectively). As seen from Fig. 6(d), the vibrations mainly comprise a rocking motion of the aromatic hydrogen and the scissoring of aldehyde group. Note that the vibronic progressions do not match the normal modes exhibiting the largest displacement between the ground and excited states, probably revealing the complexity of the vibronic coupling and the relevant vibrational wavefunction overlaps.

In order to further examine the accuracy of theoretical emission energies in comparison with the experimental spectra, exchange-correlation functionals beyond B3LYP including PBE0, CAM-B3LYP, M06-2X and wB97XD are employed. As visualized in Fig. 7, for both molecules, emissive energies adopting the hybrid functionals with lower Hartree-Fock (HF) fractions (B3LYP and PBE0) demonstrate more accurate estimations for the experimental counterparts. While functionals with higher HF fraction (like M06-2X) or others with long-range corrections (CAM-B3LYP and wB97XD) give rise to overestimations of energies. The results are compatible with previous reports [29] that PBE0-like functionals can lead to lower prediction error for emission characteristics.

These findings illuminate the critical interplay between experimental observations and theoretical computations in understanding the fluorescent behaviours of solvated molecules. The compatibility of the main features between experimental and theoretical spectra further confirms the integrity of the molecular structures as designed to possess targeted photophysical properties, and the deviations in detailed characteristics may necessitate the improvement of the theory.

3.4. PL lifetime and quantum yield

As shown in Fig. 8, the transient photoluminescence decay profiles of molecules mol_12 and mol_16 dissolved in different solvents — toluene, chloroform, and hexane — have been examined to elucidate their excited-state dynamics. For both molecules, the decay profiles are indicative of a combination of the fast and slow decay processes, clearly demonstrating the prompt and delayed fluorescence behaviours. In toluene and chloroform, mol_12 and mol_16 exhibit a rapid initial decay, followed by a slower exponential tail, implying a significant delayed component due to the reverse intersystem crossing. Conversely, in hexane, the decay profiles appear more uniform especially for mol_12, dictating an extended excited-state lifetime and a smaller discrepancy between the fast and slow components. The reason behind may be ascribed to reduced solvent interaction due to hexane's nonpolar nature, which can cause modulations of the electronic structure.

Furthermore, the comparative decay analysis between mol_12 and mol_16 unveils molecular characteristics impacting the PL decay pathways. Specifically, the sharper initial decay in mol_16 across toluene and chloroform might imply a more efficient non-radiative decay process or a faster internal conversion compared to mol_12. These observations underscore the intrinsic molecular differences affecting the emissive properties of mol_12 and mol_16 under the solvent environment.

Table 2 presents the lifetimes fitted from the PL decay profiles of mol_12 and mol_16 using the dual-exponential decay function. Obviously, both molecules show a fast decay with nanosecond lifetime and a slow decay with microsecond lifetime, similar to most of the TADF compounds reported before [25,26]. For mol_16, the prompt decay lifetimes in toluene and chloroform are relatively short, at 0.05 and 0.1 μs, respectively, which may be attributed to the efficient non-radiative decay mechanisms. Interestingly, in the non-polar solvent hexane, the PL lifetime of mol_12 extends significantly to 5.97 μs, suggesting a pronounced stabilization of the excited state. This could be due to reduced solvent interaction and the particular molecular configuration, probably leading to an intersystem quenching of the thermal activation. In contrast, mol_16 exhibits a universally short lifetime across all solvents, with a slight increase in non-polar hexane.

In order to evaluate the luminescence efficiency of fluorophores in solutions, we also measure the absolute PL quantum yield (PLQY) using an integrating sphere. A noticeable PLQY around 9.9 % in chloroform for mol_12 is found compared to the quantum yield in other two solutions which is less significant. For mol_16, the PLQY can approach 19.8 % in toluene, showing enhanced luminescence efficiency in this moderately polar solvent. Note that the minimized ΔE_{ST} (0.0084 eV) for mol_12 does not guarantee an improved photoluminescent performance, probably indicating that the rate of TADF reveals a complex interplay between vibronic and spin-orbital couplings rather than solely an energy-defined thermal process [27,28].

For a short summary, the current measurements emphasize the analysis of luminescence properties in solution phases, unveiling noticeable delayed fluorescence behaviours and quantum yield for molecules; but still lack the performance investigations at the thin film levels. It is noted that the emissive efficiencies in condensed states may be influenced by the Aggregation-Caused Quenching (ACQ) and Aggregation-Induced Emission (AIE) effects of fluorophores, which can cause uncertainties in performances at device levels. We therefore claim the feasibility of the proposed ML methodology in producing reasonable TADF molecules with verifiable

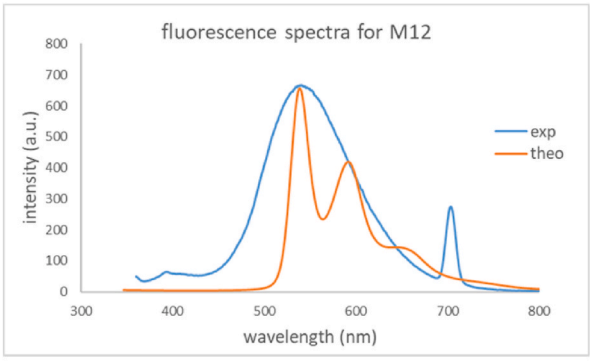

(a)

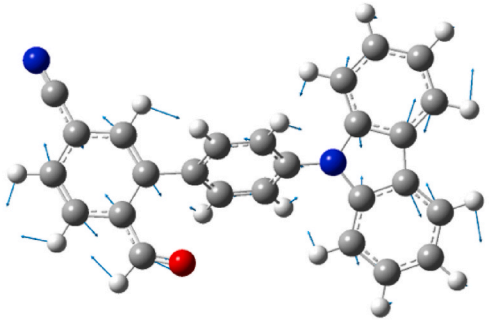

(b)

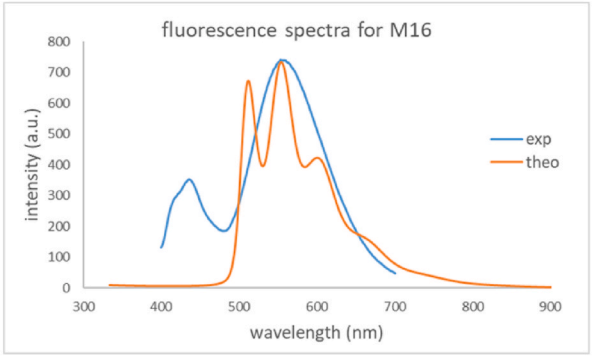

(c)

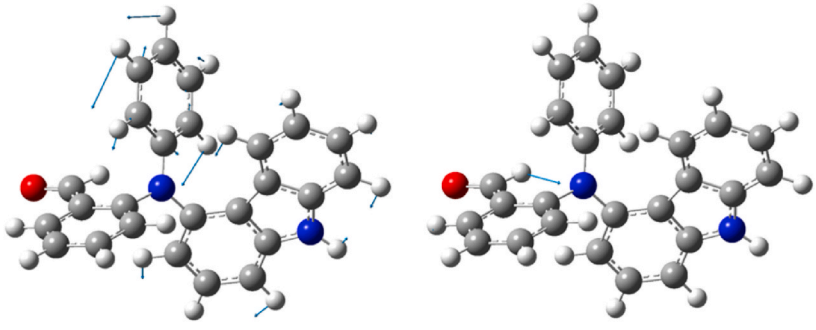

(d)

(caption on next page)

Fig. 6. Experimental and theoretical fluorescence spectra for (a) mol_12 and (c) mol_16 dissolved in Chloroform. (b) and (d) display the normal modes associated with the vibronic progression for mol_12 and mol_16 respectively. Note that the theoretical spectra are calculated with the conductor-like polarizable continuum model (C-PCM) [23] to approximate the solvation effect.

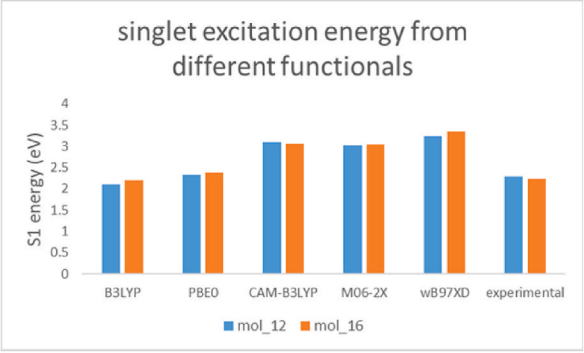

Fig. 7. S_1 emission energies at S_1 geometries for mol_12 and mol_16. The theoretical energies are calculated with the def2SVP basis set using functionals of B3LYP, PBE0, CAM-B3LYP, M06-2X and wB97XD. The experimental values are extracted from the peak positions of emission spectra. The solvation effect is involved in all calculations.

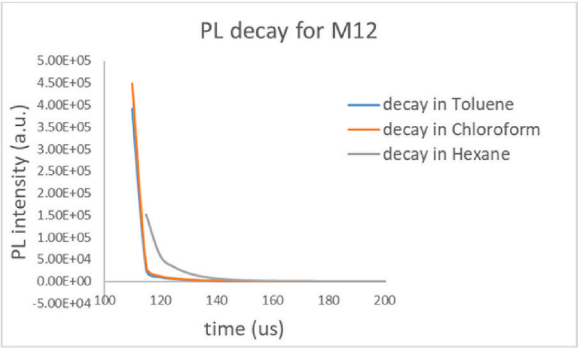

(a)

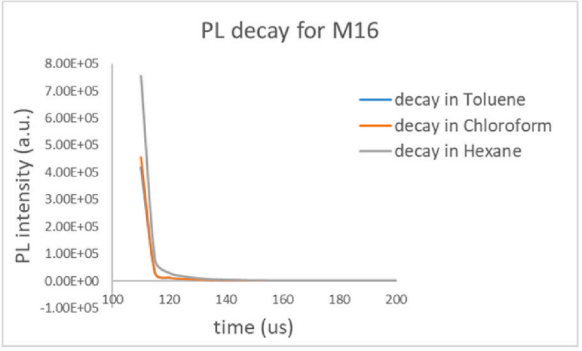

(b)

Fig. 8. Transient PL decay curves for (a) mol_12 and (b) mol_16 dissolved in toluene, chloroform and hexane respectively.

Table 2
Lifetimes fitted from the transient PL decay profiles for mol_12 and mol_16 dissolved in toluene, chloroform and hexane respectively.

PL lifetime in different solutions (μs)		Toluene	Chloroform	Hexane
mol_12	fast component	0.1	0.12	0.15
	slow component	1.81	1.89	5.97
mol_16	fast component	0.05	0.1	0.2
	slow component	1.84	1.81	2.18

photoluminescent characteristics in both gaseous and solution phases, with the potentials of applicability in OLED devices to be examined in the future.

4. Conclusions

This paper delineates the successful integration of machine learning models within the domain of materials science to expedite the design, synthesis and characterization of TADF molecules. The research offers a compelling narrative of the symbiotic relationship between computational predictions and empirical methodologies in advancing the development of TADF compounds, which are instrumental to the enhancement of OLED technology. The machine learning and high throughput screening approaches, coupled with high-precision synthetic methods, yielded a series of novel TADF molecules. The subsequent rigorous structural and performance assessments, through techniques including NMR, PL spectroscopy, transient PL decay and PL quantum yield measurement, affirmed the structural integrity and notable emission efficiencies of the synthesized molecules in solution phases, thereby validating the predictive prowess of the ML models. The findings indicate a considerable delayed component in fluorescence behaviours and a non-negligible quantum yield, further verifying the robustness of machine learning in designing TADF species with desirable photophysical properties (the statement applies to both of the synthesized molecules). In conclusion, the current work not only provides a scalable blueprint for TADF molecule development but also exemplifies the potential of machine learning to drive the intelligent advancement of display technologies.

CRediT authorship contribution statement

Weimei Shi: Writing – original draft, Methodology, Investigation, Funding acquisition. **Yan Li:** Writing – original draft, Visualization, Formal analysis, Data curation. **Ziying Zhang:** Validation, Software, Formal analysis. **Zheng Tan:** Writing – review & editing, Supervision, Project administration, Funding acquisition. **Shiqing Yang:** Resources, Conceptualization.

Declaration of competing interest

The authors declare that they have no known competing financial interests or personal relationships that could have appeared to influence the work reported in this paper.

Acknowledgement

The work is supported by the Open Foundation of State Key Laboratory of Electronic Thin Films and Integrated Devices (No: KFJJ202205); Research Platform Foundation of Chengdu Polytechnic (No: 20KYTD07); Foundation of Chengdu Polytechnic (No: 21CZYG020).

Appendix A. Supplementary data

Supplementary data to this article can be found online at https://doi.org/10.1016/j.heliyon.2024.e40750.

References

[1] C. Tu, W. Huang, S. Liang, K. Wang, Q. Tian, W. Yan, Combining machine learning and quantum chemical calculations for high-throughput virtual screening of thermally activated delayed fluorescence molecular materials: the impact of selection strategy and structural mutations, RSC Adv. 12 (2022) 30962–30975, https://doi.org/10.1039/D2RA05643G.
[2] H. Uoyama, K. Goushi, K. Shizu, H. Nomura, C. Adachi, Highly efficient organic light-emitting diodes from delayed fluorescence, Nature 492 (2012) 234–238, https://doi.org/10.1038/nature11687.
[3] M.Y. Wong, E. Zysman-Colman, Purely organic thermally activated delayed fluorescence materials for organic light-emitting diodes, Adv Mater 29 (2017) 1605444, https://doi.org/10.1002/adma.201605444.
[4] D.S.M. Ravinson, M.E. Thompson, Thermally assisted delayed fluorescence (TADF): fluorescence delayed is fluorescence denied, Mater. Horiz. 7 (2020) 1210, https://doi.org/10.1039/D0MH00276C.
[5] S.P. Huang, Q.S. Zhang, Y. Shiota, T. Nakagawa, K. Kuwabara, K. Yoshizawa, C. Adachi, Computational prediction for singlet- and triplet-transition energies of charge-transfer compounds, J Chem. Theory Comput. 9 (2013) 3872–3877, https://doi.org/10.1021/ct400415r.
[6] Z.Y. Yang, Z. Mao, Z.L. Xie, Y. Zhang, S.W. Liu, J. Zhao, J.R. Xu, Z.G. Chi, M.P. Aldred, Recent advances in organic thermally activated delayed fluorescence materials, Chem. Soc. Rev. 46 (2017) 915, https://doi.org/10.1039/C6CS00368K.
[7] X. Liang, Z.L. Tu, Y.X. Zheng, Thermally activated delayed fluorescence materials: towards realization of high efficiency through strategic small molecular design, Chem. Eur J. 25 (2019) 5623–5642, https://doi.org/10.1002/chem.201805952.
[8] A. Ramin, Computational Molecular Design for Developing Metal-free Organic Emissive Materials, University of Michigan, 2022, https://doi.org/10.7302/4729.
[9] R.G. Bombarelli, J.A. Iparraguirre, T.D. Hirzel, D. Duvenaud, D. Maclaurin, M.A.B. Forsythe, H.S. Chae, M. Einzinger, D.G. Ha, T. Wu, G. Markopoulos, S. Jeon, H. Kang, H. Miyazaki, M. Numata, S.H. Kim, W.L. Huang, S.I. Hong, M. Baldo, R.P. Adams, A.A. Guzik, Design of efficient molecular organic light-emitting diodes by a high-throughput virtual screening and experimental approach, Nat. Mater. 15 (2016) 1120–1127, https://doi.org/10.1038/nmat4717.
[10] T. Hatakeyama, K. Shiren, K. Nakajima, S. Nomura, S. Nakatsuka, K. Kinoshita, J.P. Ni, Y. Ono, T. Ikuta, Ultrapure blue thermally activated delayed fluorescence molecules: efficient HOMO–LUMO separation by the multiple resonance effect, Adv. Mater. 28 (2016) 2777, https://doi.org/10.1002/adma.201505491.

[11] S.D. Griesemer, Y. Xia, C. Wolverton, Accelerating the prediction of stable materials with machine learning, Nat Comput Sci 3 (2023) 934–945, https://doi.org/10.1038/s43588-023-00536-w.
[12] W. Xia, L. Tang, H. Sun, C. Zhang, K. Ho, G. Viswanathan, K. Kovni, C. Wang, Accelerating materials discovery using integrated deep machine learning approaches, J. Mater. Chem. A. 11 (2023) 25973–25982, https://doi.org/10.1039/D3TA03771A.
[13] Z. Tan, Y. Li, Z.Y. Zhang, T. Penfold, W.M. Shi, S.Q. Yang, W.L. Zhang, A deep learning framework for predictions of excited state properties of light emissive molecules, New J. Chem. 47 (2023) 9550–9554, https://doi.org/10.1039/D3NJ01174G.
[14] Z. Tan, Y. Li, Z.Y. Zhang, X. Wu, T. Penfold, W.M. Shi, S.Q. Yang, Efficient adversarial generation of thermally activated delayed fluorescence molecules, ACS Omega 7 (2022) 18179–18188, https://doi.org/10.1021/acsomega.2c02253.
[15] K.C. Nicolaou, P.G. Bulger, D. Sarlah, Palladium-catalyzed cross-coupling reactions in total synthesis, Angew. Chem. Int. Ed. 44 (2005) 4442–4489, https://doi.org/10.1002/anie.200500368.
[16] F. Proutiere, F. Schoenebeck, Solvent effect on palladium-catalyzed cross-coupling reactions and implications on the active catalytic species, Angew. Chem. Int. Ed. 50 (2011) 8192–8195, https://doi.org/10.1002/anie.201101746.
[17] H. Lebel, C. Ladjel, L. Bréthous, Palladium-catalyzed cross-coupling reactions in one-pot multicatalytic processes, J. Am. Chem. Soc. 129 (2007) 13321–13326, https://doi.org/10.1021/ja0733235.
[18] P. Devendar, R. Qu, W. Kang, B. He, G. Yang, Palladium-catalyzed cross-coupling reactions: a powerful tool for the synthesis of agrochemicals, J. Agric. Food Chem. 66 (2018) 8914–8934, https://doi.org/10.1021/acs.jafc.8b03792.
[19] C.Y. Legault, Y. Garcia, C.A. Merlic, K.N. Houk, Origin of regioselectivity in palladium-catalyzed cross-coupling reactions of polyhalogenated heterocycles, J. Am. Chem. Soc. 129 (2007) 12664–12665, https://doi.org/10.1021/ja075785o.
[20] M.J. Frisch, et al., Gaussian 16, Revision A.03, Gaussian, Inc., Wallingford CT, 2016.
[21] F. Neese, The ORCA program system, Wires Comput Mol Sci 2 (2012) 73–78, https://doi.org/10.1002/wcms.81.
[22] T.J. Penfold, E. Gindensperger, C. Daniel, C.M. Marian, Spin-vibronic mechanism for intersystem crossing, Chem. Rev. 118 (2018) 6975–7025, https://doi.org/10.1021/acs.chemrev.7b00617.
[23] V. Barone, M. Cossi, Quantum calculation of molecular energies and energy gradients in solution by a conductor solvent model, J. Phys. Chem. A. 102 (1998) 1995–2001, https://doi.org/10.1021/jp9716997.
[24] C. Lu, Q. Liu, Q. Sun, C. Hsieh, S. Zhang, L. Shi, C. Lee, Deep learning for optoelectronic properties of organic semiconductors, J. Phys. Chem. C 124 (2020) 7048–7060, https://doi.org/10.1021/acs.jpcc.0c00329.
[25] T. Takahashi, K. Shizu, T. Yasuda, K. Togashi, C. Adachi, Donor-acceptor-structured 1,4-diazatriphenylene derivatives exhibiting thermally activated delayed fluorescence: design and synthesis, photophysical properties and OLED characteristics, Sci. Technol. Adv. Mater. 15 (2014) 034202, https://doi.org/10.1088/1468-6996/15/3/034202.
[26] Q. Zhang, J. Li, K. Shizu, S. Huang, S. Hirata, H. Miyazaki, C. Adachi, Design of efficient thermally activated delayed fluorescence materials for pure blue organic light emitting diodes, J. Am. Chem. Soc. 134 (2012) 14706–14709, https://doi.org/10.1021/ja306538w.
[27] T.J. Penfold, F.B. Dias, A.P. Monkman, The theory of thermally activated delayed fluorescence for organic light emitting diodes, Chem. Commun. 54 (2018) 3926–3935, https://doi.org/10.1039/C7CC09612G.
[28] J. Eng, T.J. Penfold, Open questions on the photophysics of thermally activated delayed fluorescence, Commun. Chem. 4 (2021), https://doi.org/10.1038/s42004-021-00533-y.
[29] C.W. Ju, H.Z. Bai, R.Z. Liu, Machine learning enables highly accurate predictions of photophysical properties of organic fluorescent materials: emission wavelengths and quantum yields, J. Chem. Inf. Model. 61 (2021) 1053–1065, https://doi.org/10.1021/acs.jcim.0c01203.